Multiscale enhancement of refrigerant falling film boiling by combining commercially enhanced tubes with nanostructures

Bradley D. Bock[a*], Dian Dickson[a] and John R. Thome[b]

This is the Post Print version of this article. The final, published version of the article can be found at: https://doi.org/10.1016/j.applthermaleng.2023.121622

[a]*Clean Energy Research Group, Department of Mechanical and Aeronautical Engineering, Faculty of Engineering, the Built Environment and IT, University of Pretoria, Pretoria, South Africa*
[b]*JJ Cooling Innovation, EPFL Innovation Park, Bâtiment A, CH-1015 Lausanne, Switzerland*

ABSTRACT

Multiscale surface structures offer the opportunity to combine the heat transfer enhancement provided by microscale structures with the dryout benefits provided by some nanostructures, which is particularly attractive for falling film evaporators, who have to prevent dryout to ensure high heat transfer coefficients can be maintained.

In this study commercially produced plain, low-finned and 3D enhanced commercially produced tubes were tested uncoated as well as coated with fibrous nanostructures that induce wicking on the surface to investigate the opportunity that multiscale enhancements might offer falling film boiling evaporators. Single tubes were heated internally by water and tested in the horizontal position with refrigerant R-134a drizzled over the outside of the tube surface at saturation temperatures of 5 and 25°C, heat fluxes from 20 to 100 kW/m^2 and film Reynolds numbers of up to 2000. The tubes tested were a roughened plain tube, a low-finned Gewa-KS tube and two different 3D enhanced tubes, an Gewa-B5 and an Turbo EHPII, that have networks of re-entrant cavities.

The uncoated 3D enhanced tubes achieved the highest heat transfer coefficients, outperforming a roughened plain tube by up to 500 %. The uncoated low-finned tube had heat transfer coefficients that were up to 140 % higher than the roughened plain tube, despite having only an 80 % larger surface area, thought to be due to bubbles sliding down the channels between the fins, increasing the surface area of the bubbles in contact with the surface and thus allowing for increased microlayer evaporation.

The application of the copper oxide coating benefitted the low-finned tube, with heat transfer enhancement of up to 60 %, possibly due to liquid wicked underneath the sliding bubbles and onto the fin tips. However, the nanocoating largely decreased the heat transfer of the roughened plain tube and the 3D enhanced tubes, thought to be due flooding of nucleation sites on the roughened tube and interference with the hydraulics of the re-entrant cavity network on the surface of the 3D enhanced surfaces.

The low-finned tube also benefitted the most from the falling film boiling heat transfer mode compared to previous pool boiling results, with heat transfer increased by up to 80 and 460 % for the uncoated and coated low-finned tube respectively, again likely due to the bubbles sliding in the fin channels under falling film conditions.

The Gewa-B5 tubes had the best dryout performance, followed by the Turbo EHPII tubes and then the low-finned Gewa-KS tube. The open pore structure of the Gewa-B5 likely aided it in dryout prevention, while the fins of the Gewa-KS are thought to have prevented lateral fluid distribution and thus worsen dryout.

The dryout performance of the tubes we not markedly improved by the nanocoating, highlighting the difficulty in improving wettability on high wetting low surface tensions fluids such as refrigerants. Microscale enhancements were thus shown to have significant influence on dryout performance, while nanoscale enhancements had little effect in this study.

Keywords: falling film evaporation; nanocoating; nanostructures; enhanced boiling; 3D enhancements; microstructures

* Corresponding author

Email address: bradley.bock@up.ac.za

Nomenclature

C	Wilson plot modifier coefficient
c_p	Specific heat capacity
D	Diameter
f	Friction factor
Γ	Film flow rate
h	Heat transfer coefficient
K	Heat transfer enhancement ratio
k	Thermal conductivity
$\dot{m}$	Mass flow rate
Pr_w	Prandtl number of heating water, $\frac{C_{p,w}\mu_w}{k_w}$
q	Heat flux
R_a	Arithmetic mean roughness
R	Thermal resistance
Re_w	Reynolds number of water in tube, $\frac{4\dot{m}_w}{\pi(D_i+D_{probe})\mu_w}$
T	Temperature
U	Overall heat transfer coefficient
x	Coordinate dimension along the length of the tube
μ	Dynamic viscosity
Subscripts	
coated	Coated with nanostructures
CuO	Surface enhancement relative to copper oxide nanocoating
ff	Falling film
h	Hydraulic
i	Inner
norm	Normalised value
o	Outer
pb	Pool boiling
probe	Heating water temperature probe
r	Refrigerant
sat	Saturated refrigerant
uncoated	Not coated with nanostructures
w	Water
wall	Tube wall

Abbreviations

DNB	Departure from Nucleate Boiling
CHF	Critical Heat Flux
CuO	Copper Oxide
HTC	Heat Transfer Coefficient
SEM	Scanning Electron Microscope

1. Introduction

Falling film and flooded evaporators are currently used in a variety of industries spanning across refrigeration, petrochemical and desalination [1], as well future uses such as organic Rankine cycles for low grade waste heat recovery [2] or solar energy generation [3]. Falling film evaporators have a number of advantages over flooded evaporators, such as reduced charge and at times improved heat transfer [4].

However, falling film evaporators do have the inherent disadvantage compared to their flooded counterparts that when there is a limited film flow rate, dry spots can form to limit the heat transfer of the evaporator tubes [4]. This can worsen to the point that critical dryout occurs where heat transfer coefficients (HTCs) substantially decrease as

film flow rate is further reduced [1]. To overcome this, typical approaches include increasing the refrigerant feed rate to ensure sufficient liquid supply, resulting in the need for refrigerant recirculation, or flooding the bottom tubes of the falling film evaporator [1]. However, this increases the refrigerant charge needed, limiting the low charge advantage that falling film evaporators have. Dryout is thus a limitation of falling film evaporators that needs to be overcome to extend the operation envelope and to reduce refrigerating pumping costs or refrigerant charge.

Nanostructures could assist in this problem with their ability to improve the wettability of surfaces and to create surfaces with the ability to wick liquids through capillary action [5, 6]. While previous studies have largely focussed on using this ability to delay the onset of critical heat flux (CHF) in pool boiling [5, 6], these properties may be advantageous to the falling film dryout problem. Convective falling film studies have shown some success with this method, with Zheng et al. [7] and Koroglu et al. [8] showing that critical dryout can be delayed through the application of nanostructures, and thus improving heat transfer at low film flow rates due to the prevention of dry spots. However, these coatings tend not to increase heat transfer under convective conditions when both coated and uncoated tubes are fully wetted, with the HTCs largely the same until dryout occurs [7, 8].

Previous falling film boiling research by this research group on plain tubes coated with nanostructures under falling film conditions of various refrigerants have also showed promise in this regard [9], with two of the tested coatings delaying the onset of critical dryout when operating at lower heat fluxes (approximately 20 kW/m^2) and showing improved dryout profiles. Furthermore, heat transfer enhancement mechanisms unique to nanostructures were noted and the accompanying pool boiling study [10] suggested this was as a result of capillary wicking of liquid through the nanostructures, resulting in single-phase superheating of liquids in the nanochannels [11] and increased microlayer evaporation underneath nucleating bubble [12].

Commercial falling film refrigerant evaporators are unlikely to use plain tubes and would rather use commercially produced enhanced tubes which have surface enhancements such as low-fins, 3D finned structures or porous structures. The low-finned tubes have been shown to increase HTCs by up to 3.5 times [13] compared to a plain tube and the 3D enhancements by up to 7 [14] to 10 times [1] that of plain tubes. Commercially produced porous tubes, manufactured from sintered copper powder, have shown to increase HTCs of up to 4 times that of a plain tube, while Ubara et al. [15] manufactured a porous coating through the application of a thermal spray on the outside of a tube and obtained HTCs of up to 4.8 times that of a plain tube under falling film boiling conditions. Enhanced condensation tubes have also been tested as they are designed to shed liquid to ensure a thin liquid layer and so a low liquid thermal resistance under condensing conditions and may similarly benefit falling film boiling conditions, but the results show that they have HTCs of similar order as 3D enhanced boiling tubes [16, 17]. These commercially available 3D enhanced tubes have also shown themselves able to improve dryout, with the interconnected pores [4, 16] and capillary forces as a result of these pores [18] thought to be the cause of this. Low-finned tubes were noted however to worsen dryout, as the fins prevent the axial distribution of the liquid [19].

Multiscale enhancements, where nanostructures are applied to the macro and micro scale commercial enhancements might thus offer the opportunity to combine the benefits of each enhancement. Multiscale enhancements have been investigated before in pool boiling studies, which have shown that at times combining nanostructures and micro/macro structures can lead to even higher HTCs than the separate enhancements alone [5, 20, 21], but at other times such combinations can be detrimental to heat transfer [21-23]. For example, a recent study by Liu et al. [24] investigated the effect of combining an array of square micro pin-fins on a silicon substrate together with nanostructures in the boiling of FC-72 under saturated and subcooled conditions. The nanostructures were applied to the entire pin fin array or selectively to either the top corners or top edges. Compared to the plain pin fin surface, the full nanostructure coated pin fin surface produced the highest HTCs at lower fluxes which was thought to be a result of increased bubble nucleation as well as increased evaporation from the side walls into the bubbles as it grows within the microchannels between the coated pin-fins.

Studies where multiscale enhancement are investigated with re-entrant cavities are rare, as a majority of multiscale enhancement studies make use of custom manufactured micro enhancements on flat plates rather than commercially produced tubes [21]. Deng et al. [25] tested re-entrant cavities with pore openings of approximately 500 μm that were manufactured from sintered copper powder with particles of between 50 to 70 μm in ethanol and water in sub-cooled pool boiling conditions. They found that these porous re-entrant cavities were able to boost HTCs by between 3 to 5.3 times that of an equivalent solid re-entrant cavity. The increased nucleation sites, enlargement of the heat transfer area and liquid replenishment of bubble nucleation due to the porous structures were the main factors thought to be behind the heat transfer improvements.

Results of testing the effects of a combination of commercial macro and microstructure enhancements together with nanostructures under falling film boiling conditions are limited in the open academic literature. Jin et al. [17] modified the surface of a plain tube as well as a boiling and condensation 3D enhanced tube with a fluoride polymer

coating in an attempt to create a hydrophobic surface to investigate the composite effects of microstructures and modified surface wettability under falling film boiling of R134a. The measured contact change as a result of the coating was noted however to be small, with contact angle tests using the fluorinert FC-72, as a substitute for R134a, showing the contact angle changed from approximately 2° to 4° and highlighting the difficulty of creating hydrophobic surfaces with low surface tension fluids such as refrigerants and fluorinerts. The plain tube and condensation tube showed minimal change to HTCs as a result of the coating. The boiling tube showed HTC improvements of between about 20 % to 60 % for the heat flux range tested (5 kW/m2 to 80 kW/m^2 at a film Reynolds number of 800). The authors attributed the HTC increase to the reduction in flow friction within the network of re-entrant cavities as a result of the low energy polymer coating allowing for the easier flow of the two-phase mixture within the cavity network and easier escape of vapour from the cavities, thus enhancing heat transfer.

This study aims to test the ability of commercially produced micro-enhanced tubes under falling film conditions to increase heat transfer and improve dryout, as well as any further improvement in heat transfer and dryout as a result of a nanostructure coating applied to the enhanced tubes under falling film boiling conditions. A roughened tube and previous polished tube results [9] were included for comparison. The tubes were investigated under saturated falling film conditions in refrigerant R-134a at 5°C in the horizontal position across a heat flux rage of 20 kW/m^2 to 100 kW/m^2 and a film flow rate range of 0 kg/m/s to 0.13 kg/m/s, which corresponds to a film Reynolds number of 0 to approximately 2000. This paper follows on from the work in Dickson et al. [26] who tested the same tubes under the same refrigerant conditions, but in a pool boiling mode of operation.

2. Experimental and tube setup

2.1. Experimental setup

A detailed description of the testing process is given in Bock et al. [27] and Bock [28] and is briefly described again here. Tubes were tested individually in the horizontal position in a test chamber under falling film boiling. R134a refrigerant was used as the boiling medium in a custom test facility and is schematically illustrated in **Figure 1**(a). A refrigerant distributor spread a thin falling film of liquid along the length of the outside of the tubes, while the tubes were heated by water flowing on the tube inside, with a custom thermocouple probe measuring the water temperature profile along the length of the tube. The saturation temperature of refrigerant on the outside of the tubes was calculated using the measured saturation pressure. The saturation temperature was also measured directly with thermocouples in the test chamber and differed by no more than 0.2°C to the theoretically calculated saturation temperature. As no wall temperatures were measured directly, a Wilson plot analysis was used to determine the internal and external HTCs. This is discussed in more detail in section 3.1.

The test chamber is fitted with large clear windows to allow for the capture of high-speed video using a Photron FASTCAM Mini UX100 high-speed video camera at 2 000 fps.

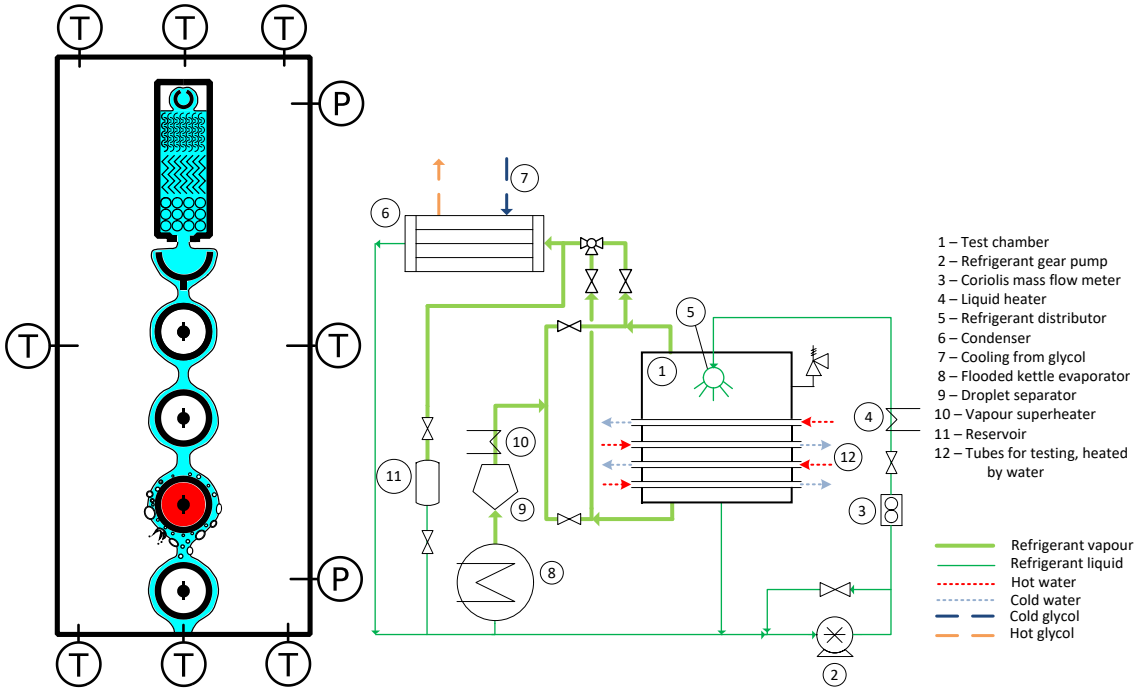

(a) Test chamber with distributor (b) Refrigerant loop with test chamber

Figure 1. Schematic of the (a) test chamber and (b) refrigerant loop (taken from Bock et al. [27])

The refrigerant used within the test chamber was conditioned through a refrigerant loop, illustrated schematically in **Figure 1**(b). Refrigerant from the test chamber flowed to the bottom of the refrigerant loop, which acted as a sump, and was then supplied via a pump (item 2) to the distributor (item 5) while being conditioned and measured. The vapour produced from the boiling process went to a glycol-cooled overhead condenser (item 6), whereafter the condensed refrigerant fell to the inlet of the refrigerant pump. The heating water used within the tubes was conditioned with a similar style loop.

2.2. Tubes tested

Four tubes of nominal 3/4" outside diameter (approximately 19 mm) were tested. A plain tube was roughened with sandpaper with a resulting roughness, R_a, of 0.75 µm, measured across the grain using a diamond tip profilometer (Mitutoyo SJ Surftest 210). A low-fin Gewa KS tube with 19 fpi was tested, as well as two 3D enhanced tubes, the Gewa B5 and the Turbo EHPII, all produced by the Wieland Group. The Gewa B5 and Turbo EHPII both have 3D enhanced fins that create a network of re-entrant cavities, but the Turbo EHPII's enhancements overlap to create a "closed-pore" scaled pattern on the surface, while the Gewa B5 has a more "open-pore" cavity structure. Schematic illustrations of these surfaces are shown in **Figure 2** and a summary of the tube characteristics as measured in this study are shown in **Table 1**.

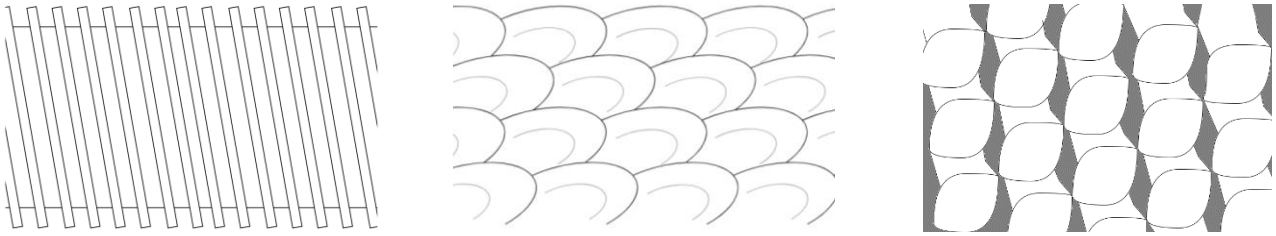

(a) Gewa KS (b) "closed-pore" Turbo EHPII (c) "open-pore" Gewa B5

Figure 2. Schematics showing a top-view of the micro enhanced surface microstructures

Table 1. Tube characteristic dimensions

Tube name	D_o (mm)	D_{or} (mm)	D_i (mm)
Plain	19.1		16.7
Gewa B5	18.8	17.4	16
Gewa KS	18.8	17.2	14.9
Turbo EHPII	18.9	18.6	16

2.3. Nanocoating of tubes

All four tubes were nanocoated through a chemical process that creates a forest of copper oxide (CuO) nanostructures on the surface of the copper tubes. All tubes were prepared and coated using identical standardised processes to ensure the same nanostructures appear on all tubes. The tubes were first cleaned with a weak acidic solution before being dipped in a heated alkaline solution to create the nanocoating, while being constantly rotated to ensure an even coating. The solution is heated to 95°C and consists of, per 100ml of deionised water, 10 g of $Na_3PO_4{\cdot}12H_2O$, 5 g of NaOH and 3.75 g of $NaClO_2$. Further details of this process and the resulting CuO nanostructures are documented in Nam and Ju [29] as the Type I nanocoating as well as in Enright et al. [30].

The SEM images shown in **Figure 3** illustrate the coating on the tubes. The CuO coated roughened plain surface in **Figure 3**(a) shows the forest of CuO nanostructures on the tube surface. The CuO coating has been shown in our previous work [10] to be between 2 to 3 μm thick and thus has a negligible influence on the wall thermal resistance, increasing it by less than 0.1%. SEM images were taken of the 3D enhanced surface to confirm that the pores are not blocked by the CuO coating. The Gewa B5 tube had unblocked pores, while the Turbo EHPII tube was shown to have some blockages (**Figure 3**(b)), but the entire pore was never seen to be blocked, with a porous webbing stretching over the pore at best. A survey of the SEM images showed that only about 10 % of pores had some form of CuO obstruction on the pores. Considering that the coating is created with an alkaline solution, it is expected that the coating will be able to penetrate the inside of the pores, and SEM images of the inside of the Gewa B5 pores confirmed that the CuO nanostructures had coated the inside of the pores consistently.

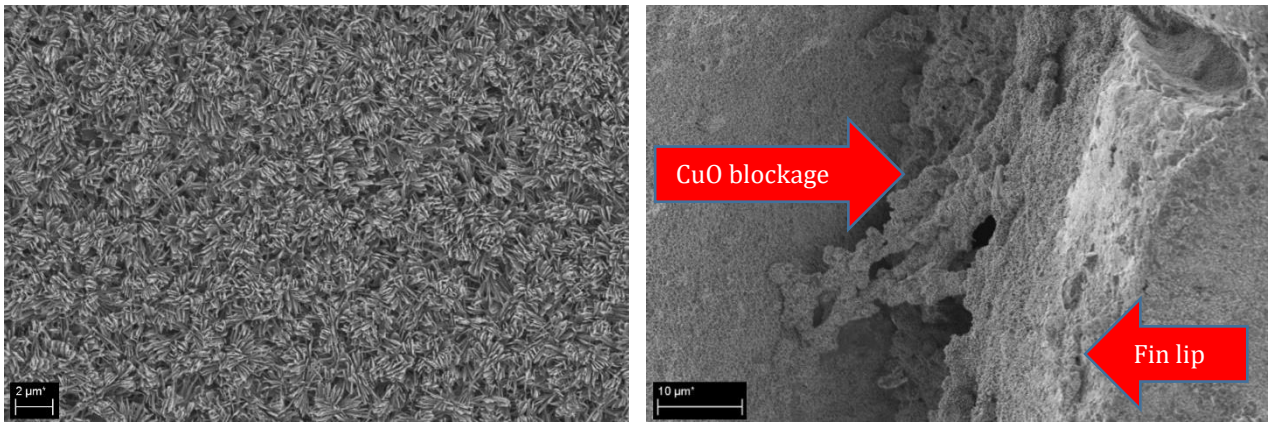

(a) CuO coated roughened plain surface (b) Blocked pore of CuO coated EHPII surface

Figure 3. SEM of the CuO nanocoated surfaces

3. Data reduction and uncertainties

A brief outline of the data reduction methodology is given here, with full details given by Bock et al. [27].

3.1. Wilson plot analysis and internal heat transfer coefficient

Since no wall temperatures were measured directly and only an overall HTC could be calculated directly from the measurements, a Wilson plot analysis was conducted to determine the external HTCs and internal HTCs. The tubes tested in this study all had different interior surfaces, with the roughened tube having a plain interior, while the Gewa KS, Gewa B5 and Turbo EHPII tubes all having various degrees of internal enhancement.

The Wilson plot analysis characterized the tubes by maintaining the external conditions of the tube at a constant pool boiling heat flux while varying the interior Reynolds number of the water. This allowed for the determination of the Wilson plot coefficient, C_i, used to modify the Gnielinski correlation [31] when determining the internal HTC, h_i, as follows

$$h_i = C_i \frac{(f/8)(Re_w - 1000)Pr_w}{1+12.7(f/8)^{0.5}(Pr_w^{2/3}-1)}\left(\frac{k_w}{D_h}\right) \quad (1)$$

where the friction factor, f, was calculated from Petukhov's correlation [32]. The Reynold's number, Re_w, and Prandlt number, Pr_w, of the heating water inside the tube were calculated using the measured water temperature at the midpoint of the tube length. The thermal conductivity, k_w, and other properties of the water were calculated using CoolProp v6.4.1 [33] . The hydraulic diameter, D_h, was given by the difference between the inner diameter of the tube, D_i, and outer diamter of the temprature probe, D_{probe}.

The Wilson plot coefficient, C_i, for each tube tested is shown in **Table 2**. As can be seen, the 3D enhanced tubes have the highest internal Wilson plot coefficient due to the advanced helical structures present in an effort to improve convective heat transfer.

Table 2. Wilson plot coefficients for tubes

Tube	Wilson plot coefficient, C_i
Plain roughed	1.28
Gewa-KS	3.91
Gewa-B5	4.20
Turbo EHPII	4.48

3.2. Local heat flux

The local heat flux at the midpoint of the tube, q, was calculated by

$$q = \frac{\dot{m}_w c_{p,w}}{\pi D_o}\frac{dT_w}{dx} \quad (2)$$

where $\dot{m}_w$ was the measured water mass flow rate, D_o was the measured outer diameter of the tube tested and dT_w/dx was the measured temperature gradient at the midpoint of the tube estimated with a second-order polynomial fit through the measured temperature profile of the water along the length of the tube. The specific heat capacity of the water, $c_{p,w}$, was theoretically obtained from CoolProp v6.4.1 [33].

3.3. External heat transfer coefficient

The external HTC of the tube at its centre point along its length, h_o, was calculated by

$$h_o = \left(\frac{1}{U_o} - R_{wall} - \frac{1}{h_i}\frac{D_o}{D_i}\right)^{-1} \quad (3)$$

where, R_{wall}, is the calculated wall thermal resistance.

The overall HTC, U_o, was calculated by

$$U_o = \frac{q}{T_w - T_{sat}} \quad (4)$$

where T_w was the measured heating water temperature at the midpoint of the tube and T_{sat} was the calculated saturation temperature of the refrigerant from CoolProp v6.4.1 [33] based on the measured saturation pressure of the refrigerant.

3.4. CuO coating factor

The influence of the CuO nanocoating was characterized by the CuO coating factor, K_{CuO}, where the HTC of the CuO coated tubes was compared relative to the HTCs of the uncoated tube under the same refrigerant conditions

$$K_{CuO} = \frac{h_{o,coated}}{h_{o,uncoated}} \quad (5)$$

where $h_{o,coated}$ is HTCs measured on the CuO tube, and $h_{o,uncoated}$ is the HTCs measured on the uncoated tubes. As the HTC of the coated and uncoated tubes were not always measured at the exact same heat flux, a polynomial was used to interpolate the HTCs of the uncoated tube to the same heat flux as that of the coated tube.

3.5. Falling film enhancement factor

The influence of the falling film conditions on the HTCs relative to the respective pool boiling conditions (documented in Dickson et al. [26]) was captured through the falling film enhancement factor, K_{ff}, given by

$$K_{ff} = \frac{h_{o,ff}}{h_{o,pb}} \quad (6)$$

where $h_{o,ff}$ is external HTC under falling film conditions and $h_{o,pb}$ is the external HTC under equivalent pool boiling conditions, with the pool boiling HTC interpolated using a polynomial fit to the same heat flux as the falling film HTC.

3.6. Normalised external heat transfer coefficient

A normalised HTC , $h_{o,fs,norm}$, was calculated for studies where the refrigerant flow rate was varied at a constant testing heat flux. The complete HTC dataset was divided by the HTC at a film flow rate, Γ_r, of 0.13 kg/m/s, as this is the highest film flow used in this study.

$$h_{o,fs,norm} = \frac{h_{o,ff}}{h_{o,ff}(\Gamma_r=0.13)} \quad (7)$$

3.7. Uncertainties

The expanded standard uncertainties of the probes were determined in accordance with Dunn [34], and the combined standard uncertainties of the calculated quantities were determined in accordance with JCGM 100:2008 [35].

The average expanded uncertainty of the temperature probes was 0.1 K, that of the pressure probes was 0.2%, that of the mass flow rate of water, $\dot{m}_w$, was 0.19 % and that of the refrigerant film mass flow rate, $\dot{m}_r$, was 0.54 %. JCGM 100:2008 [35] was used to calculate the combined standard uncertainties of the calculated quantities through the law of propagation of uncertainty. These uncertainties varied across the heat flux range and are summarised in **Table 3** for the roughened plain tube and Gewa B5, illustrating the range of uncertainties across the test matrix.

Table 3. Summary of uncertainties

	Roughened tube			Gewa B5		
	Overall average uncertainty [%]	Average uncertainty at 20 kW/m² [%]	Average uncertainty at 100 kW/m² [%]	Overall average uncertainty [%]	Average uncertainty at 20 kW/m² [%]	Average uncertainty at 100 kW/m² [%]
q	14.4	15.5	7.1	8.6	17.6	4.0
h_o	30.3	35.5	26.4	28.3	62.2	13.6
K_{CuO}	5.9	14.6	4.3	10.6	22.6	6.8

4. Results and discussion

4.1. Heat transfer coefficients

Uncoated tubes

The measured external HTCs, h_o, on the outside of the uncoated tubes tested at saturation temperatures of 5 and 25°C are illustrated in **Figure 4**. The film flow rate was maintained at 0.13 kg/m/s for these results to minimise the influence of dryout on the results.

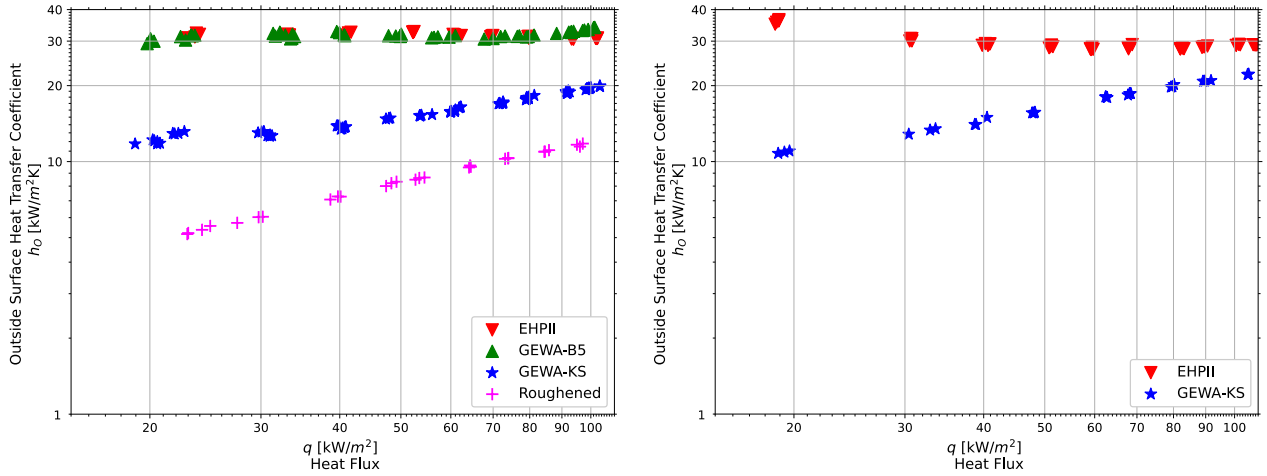

(a) 5°C (b) 25°C

Figure 4. The heat transfer performance of uncoated tubes as a function of heat flux at 5°C and 25°C saturation temperature at a film flow rate of 0.13 kg/m/s.

The Turbo EHPII and Gewa-B5 tubes showed nearly identical HTCs at 5°C and outperformed the Gewa-KS tube by between approximately 150 % to 60 % and outperformed the roughened tube by between approximately 500 % to 160 %. The Turbo EHPII outperformed the Gewa-KS by between approximately 250 % to 40 % at 25°C. This performance is to be expected, as this is the primary objective of the Turbo EHPII and Gewa-B5 tubes. The 3D enhanced tubes, with re-entrant cavities that are interlinked to form a microporous network, enhance the heat transfer performance through a variety of mechanisms, such as increased nucleation site density, thin film evaporation and single phase convection with the porous network [11].

The Gewa-KS tube outperformed the roughened tube by between 140 % to 70 % across the heat flux range. The Gewa-KS tube is a low-finned tube with a surface area approximately 80 % larger than that of the roughened tube. Thus, besides its larger surface area, the Gewa-KS enhances heat transfer through another mechanism. It is proposed that bubbles are trapped in the channels between the fins and slide down in the falling film, allowing for increased thin film evaporation as three sides of the boxed-in bubbles are in contact with the surface as it slides down channels between fins. This also ties in with the results presented shortly in Section 4.3, where the Gewa-KS HTCs under falling film conditions outperform those achieved under pool boiling, and it is discussed further there.

The roughened and Gewa-KS tube HTCs are seen in increase linearly on the log-log plot at both 5°C and 25°C with a similar gradient in both instances. This is typical of these uncomplicated surfaces, where increases in heat flux increase the nucleation site density at a constant rate.

The Turbo EHPII and Gewa-B5 tube both displayed constant HTCs at 5°C, and at 25°C the Turbo EHPII tube was moderately constant, except at the lowest heat flux of 20 kW/m^2 where an increase in HTC was seen. This insensitivity to heat flux has been noted before on 3D enhanced tubes [36-38] , with internal cavity dryout as heat flux is increased often thought to be the cause of it.

The increased HTC of the Turbo EHPII tube at 20 kW/m^2 at 25°C is an interesting case and might point to a falling film enhancement effect, as a similar HTC boost was not seen in the equivalent pool boiling study [26]. This and other falling film enhancement effects will be discussed in further detail in section 4.3 of this paper.

CuO coated tubes

The HTCs of the plain and enhanced tubes with a CuO coating applied are illustrated in **Figure 5** across a range of heat fluxes at 5°C and 25°C respectively, at a film flow rate of 0.13 kg/m/s.

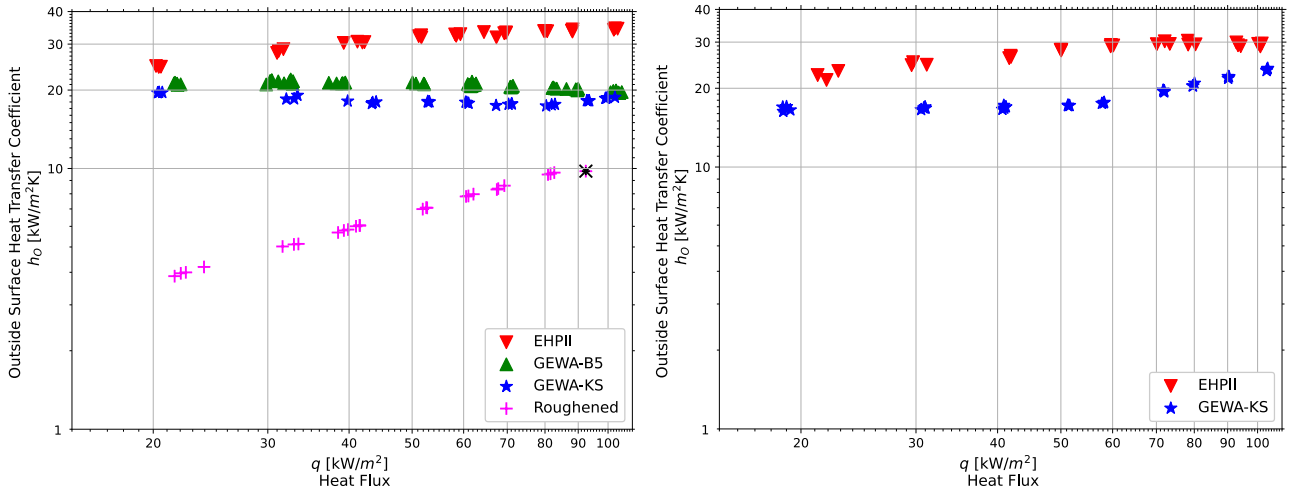

(a) 5°C (b) 25°C

Figure 5. The heat transfer performance of CuO coated plain and enhanced tubes as a function of heat flux at 5 and 25°C saturation temperature at a film flow rate of 0.13 kg/m/s.

The coated tubes showed the same order of performance at 5°C and 25°C, with the Turbo EHPII tube performing the best, followed by the Gewa-B5, Gewa-KS and the roughened tube. However, at 5°C, the coated Gewa-B5 and coated Gewa-KS HTCs were now similar. The CuO coating thus influenced the heat transfer performance of these two tubes significantly. At 25°C, the coated Turbo EHPII tube still outperformed the Gewa-KS tube, although the difference between the two tubes decreased, as the Gewa-KS tube's HTCs were increased by the coating.

The CuO coating also influenced the sensitivity of the Gewa-KS tube to changes in heat flux, as it, together with the coated Turbo EHPII and coated Gewa-B5 tubes, all displayed flat heat transfer profiles as heat flux was increased at both 5°C and 25°C.

Section 4.2 will further analyse and discuss the CuO coating's impact on the tubes.

It should be noted that the CuO coated roughened tube in this study could not be tested at heat fluxes greater than 90 kW/m², as departure from nucleate boiling (DNB) critical heat flux (CHF) was initiated and is indicated by the star in **Figure 5**. This DNB is illustrated in **Figure 6** at 100 kW/m², and while the uncoated tube is unaffected in **Figure 6** (a), in **Figure 6** (b) the bottom of the coated roughened tube is experiencing the first signs of liquid film lift off. This DNB is low if compared to a uncoated plain tube under pool boiling conditions, as the DNB is predicted to be 324 kW/m² by Lienhard and Dhir [39]. However, this DNB CHF is of similar magnitude to the DNB recorded on a CuO coated polished plain tube in a previous study by this research group of 189 kW/m² under pool boiling conditions [10], and 108 kW/m² under falling film boiling conditions [9]. The CuO coating has thus now been shown in multiple studies to cause the early onset of DNB. As suggested in Bock et al. [10] this early onset of DNB may be caused by the nanostructures trapping the vapour of the refrigerant at higher heat fluxes resulting in a Cassie-Baxter wetting state.

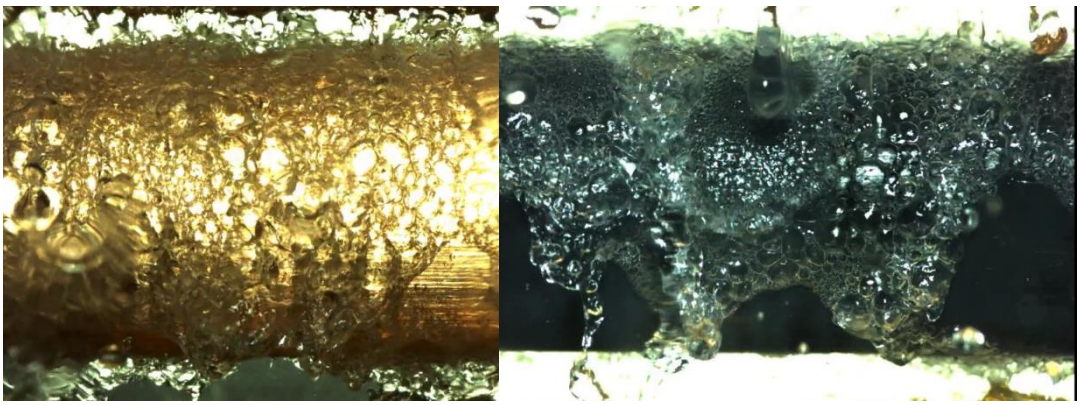

(a) Uncoated (b) Coated

Figure 6. Roughened tube at 100 kW/m^2 and 0.13 kg/m/s, illustrating film lift off DNB of the coated tube at the bottom of the tube

4.2. Influence of CuO coating on heat transfer performance

The influence of the CuO coating on the heat transfer performance of the tubes is captured through the CuO enhancement factor illustrated in **Figure 8** at 5°C and 25°C saturation temperatures, at a film flow rate of 0.13 kg/m/s.

The CuO coating was shown to decrease the HTCs of the roughened tube by between approximately 10 % to 20 %. This may be due to a reduction in nucleation site density, with the coating's increased wettability flooding some nucleation sites. However, considering that the difference between this studies uncoated tube HTCs and the comparative results from Bock et al. [27] with the same roughness tubes are also between approximately 10 % to 20 %, and taking the uncertainty of the results into account, the difference is not significant.

The CuO coating reduced the heat transfer performance of the Gewa-B5 tube by approximately 30 % to 40 % and the Turbo EHPII tube by up to 20 % at lower heat fluxes. The coating is thought to have interfered with the complex vapour and fluid flow dynamics within the network of re-entrant cavities that make up the surface of these 3D enhanced tubes. It is hypothesized that it is through the rough surface the CuO coating creates within the microcavities and the subsequent increased pressure drop and reduced fluid flow that reduces the single-phase enhanced heat transfer through these channels. This hypothesis aligns to the findings of Jin et al. [17], who found a polymeric coating applied to 3D enhanced tubes increased heat transfer, thought in that case to be as a result of decreased pressure drop in the microcavities due to the smooth polymeric coating.

As illustrated in **Figure 7**, the inspection of the boiling process was very challenging. This is due to the complex surface structure of the enhanced tubes, the boiling process itself and the black surface of the CuO coating interfering with the lighting. The coating may also therefore interfere with the bubble release dynamics from the re-entrant cavities and reduce the bubble's ability to pump liquid through the network of cavities, but this was unconfirmed in this study.

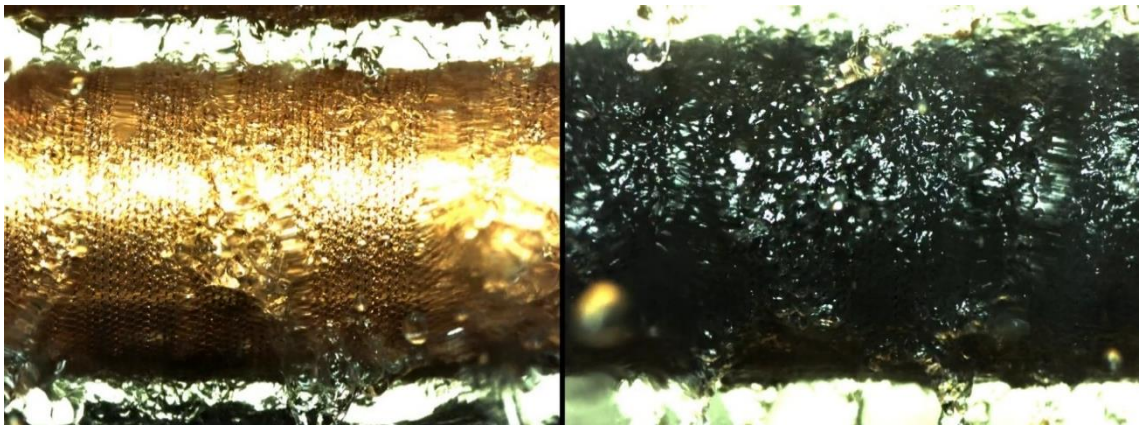

(a) Uncoated (b) Coated

Figure 7. Boiling process on the Gewa B5 at 100 kW/m^2 and 0.13 kg/m/s.

The Turbo EHPII tube HTCs were boosted by the coating at heat fluxes above 60 kW/m^2 at both saturation temperatures by up to 10 %, possibly through reduced internal dryout because of the CuO coating.

Any theorized mechanisms that would have allowed the CuO coating to have further boosted the heat transfer such as those identified by Bock et al. [10], which include the wicking of liquid underneath nucleating bubbles to increase the bubbles' evaporative heat flux, appear to not have occurred, or where overwhelmed by the associated negative effects the CuO coating had on the hydrodynamics of the fluid flow within the re-entrant cavity network.

Although the coating tested in this study had a largely negative effect on heat transfer when applied to already microenhanced tubes, considering the large selection of coatings available that can change surface properties, others may offer better results. However, care must be taken when using any coatings that produce structures with high relative roughness, as these are expected to reduce heat transfer on 3D enhanced tubes due to the increased friction caused within the microchannel network and subsequent disruption of bubble induced single phase flow within.

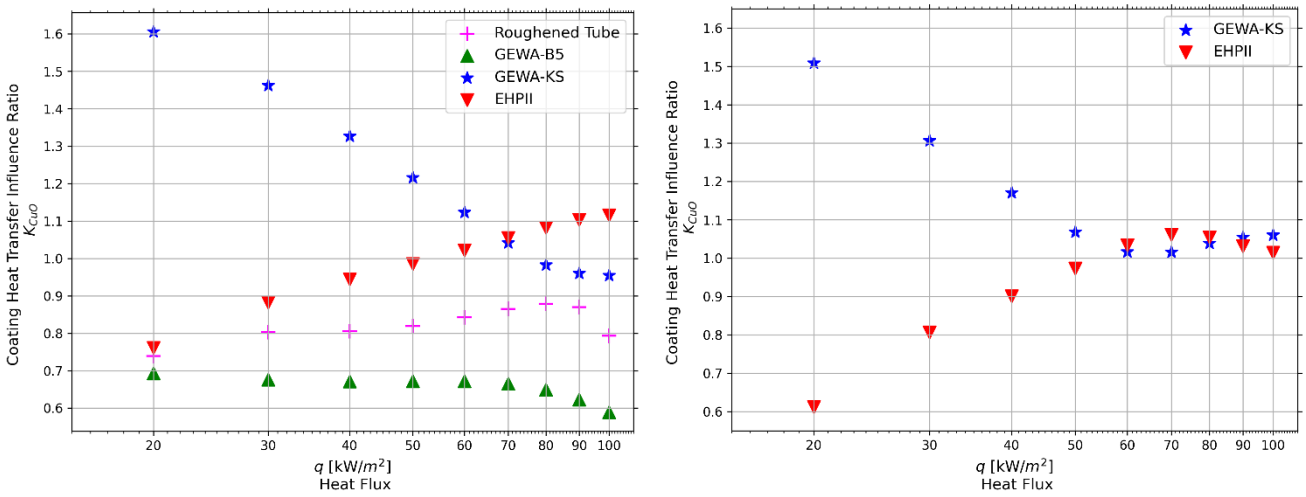

(a) 5°C (b) 25°C

Figure 8. The CuO enhancement factor, at 5 and 25°C saturation temperatures at a film flow rate of 0.13 kg/m/s.

The Gewa-KS tube was the only tube to benefit from the CuO coating, particularly at low heat fluxes, with the HTC enhancement reaching as high as 60 % at 5°C. Given that the respective pool boiling results did not show any heat transfer improvement when coating the Gewa-KS with the CuO nanostructures [26], it can be safely assumed that the heat transfer advantages gained by the Gewa-KS in this study are specific to the falling film mode of operation in this study. The low-finned enhancements of the Gewa-KS may thus have benefited from the wickabilty of the coating allowing for liquid to possibly be wicked underneath the sliding bubbles, increasing thin film evaporation, and to be spread out onto the very tips of the fins, reducing fin-tip dryout and thus increasing the surface area of the fins that were used for heat transfer, as well as possibly allowing for thin film evaporation on the fin-tips. High speed video taken of the process was not able to definitely support or disprove these theories however.

4.3. Comparison to pool boiling

Figure 9 compares the heat transfer performance of the uncoated and coated tubes tested in this study at 5°C under falling film boiling conditions to the pool boiling heat transfer performance of the same tubes under the same condition recorded in Dickson et al. [26] through the falling film enhancement factor, K_{ff}.

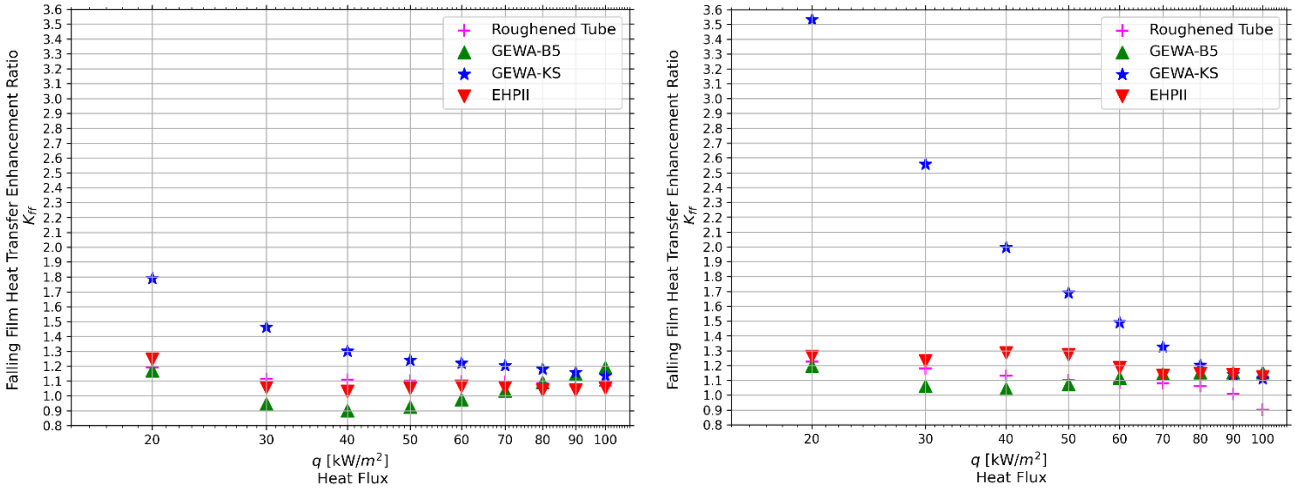

(a) Uncoated (b) Coated

Figure 9. The falling film enhancement factor at 5°C saturation temperature at a film flow rate of 0.13 kg/m/s

The performance of the roughened, Turbo EHPII and Gewa-B5 tubes under falling film boiling conditions was all similar when compared to the respective pool boiling performance both for uncoated and coated tubes at 5°C, with the falling film HTCs of all three tubes approximately 10 to 20 % higher than the pool boiling HTCs at the lower and higher fluxes respectively. This is a similar performance to previous studies conducted on plain tubes and micro or nano enhanced tubes [9, 27, 40, 41]. The cause of the falling film HTC enhancement is thought to be the same thus for all these different surfaces, namely that falling film heat transfer is boosted by the increased microlayer evaporation

underneath bubbles trapped in the falling film sliding down the tube surface compared to the pool boiling bubbles that escape from the surface. This mechanism's contribution to total heat transfer diminishes as heat flux is increased, with the higher heat fluxes resulting in boiling dominant heat transfer.

The Gewa-KS tube showed the greatest benefit from operating under falling film boiling conditions, particularly at lower heat fluxes. The uncoated Gewa-KS had a maximum increase in HTCs of 1.8 times those of pool boiling at the lower heat flux 20 kW/m^2, with this advantage decreasing as heat flux was increased until only a 1.2 times improvement at was seen 100 kW/m^2. Chien and Tsai [13] also documented the advantage a low-fin tube gains from falling film conditions, with a falling film enhancement factor as high as 5 at approximately 5 kW/m^2 in R-245fa. For the results in this study, it was noted that bubbles generated would break up into smaller bubbles that were roughly the size of the channel gaps between the fins, as seen in **Figure 10** (a), and can be seen sliding down between these channels formed by the fins. The bubbles are thus boxed in on three sides by the fin channels, illustrated in **Figure 10** (b). These sliding bubbles thus have an increased contact area with the surface of the tubes and the increased microlayer evaporation underneath these sliding bubbles is thus thought to cause this improved falling film boiling performance compared to pool boiling.

The coated Gewa-KS showed an even greater affinity for falling film boiling, with a maximum of 3.6 times the heat transfer of the respective pool boiling case at 20 kW/m^2. Combined with the same increased microlayer evaporation underneath sliding bubbles within the fin channels as experienced by the uncoated Gewa-KS, the coated Gewa-KS may have further benefitted from the CuO allowing for even greater microlayer evaporation underneath the sliding bubbles by wicking liquid underneath the bubbles, or wicking liquid to the fin tips, allowing for thin film evaporation at the fin tips to contribute meaningfully at the lower heat fluxes tested.

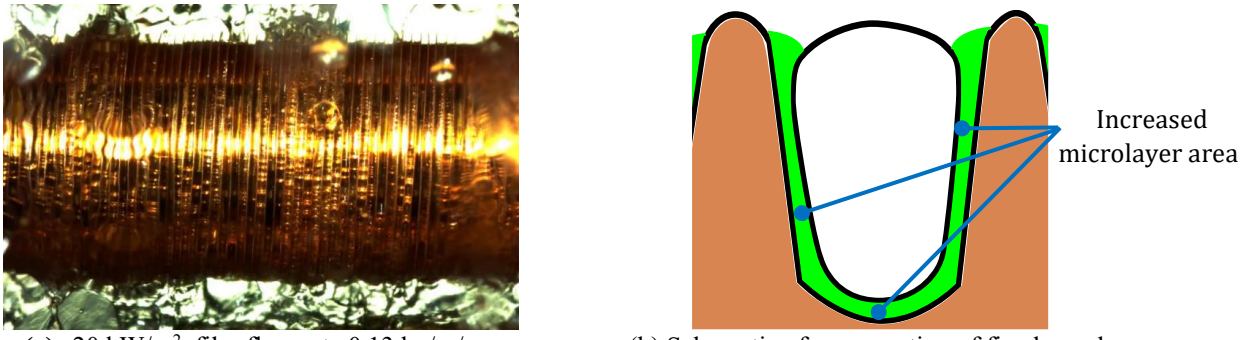

(a) 20 kW/m^2, film flow rate 0.13 kg/m/s. (b) Schematic of cross section of fin channel

Figure 10. Falling film boiling process on low-fin Gewa KS tube

Figure 11 shows the falling film enhancement factor for those tubes tested at 25°C. The Turbo EHPII tube, both uncoated and coated, showed a similar falling film enhancement at 25°C as was seen at 5°C, with the enhancement between 10 % to 30 %.

The Gewa-KS again at 25°C showed the greatest falling film enhancement, but the enhancement was less than that seen at 5°C. The uncoated Gewa-KS tube in particular did not benefit greatly from the falling film boiling mode at 25°C, with enhancements of only between 10 % to 20 %. The CuO coated Gewa-KS tube benefitted from the falling film boiling mode by between 10 % to 130 % across the range of heat fluxes tested.

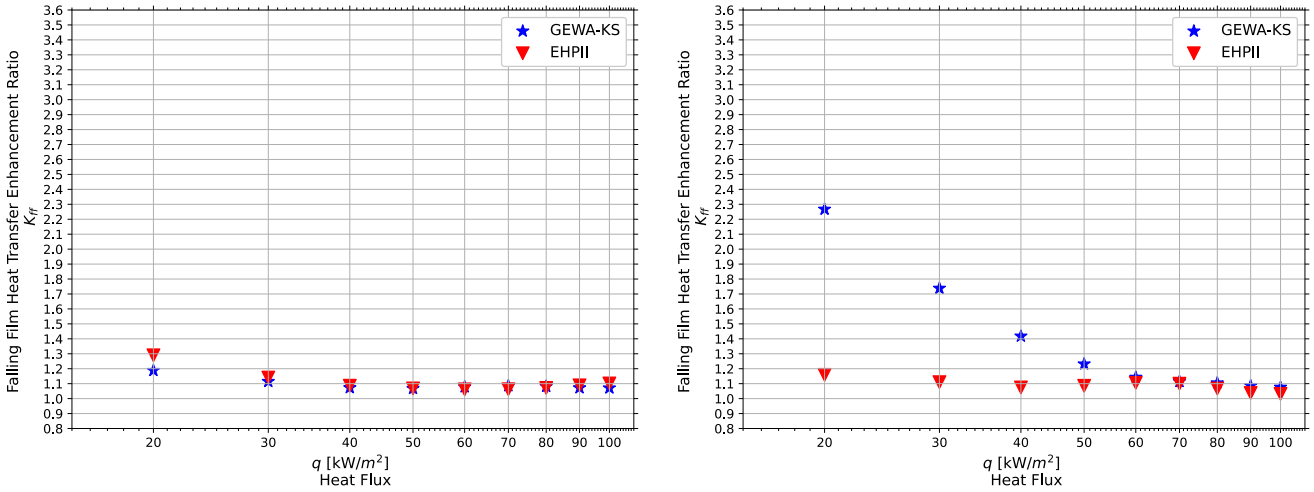

(a) Uncoated (b) Coated

Figure 11. The falling film enhancement factor at 25°C saturation temperature and a film flow rate of 0.13 kg/m/s

4.4. Dryout

The dryout performance of each tube, both uncoated and coated, was characterised by decreasing the film flow rate from a high of 0.13 kg/m/s to as low as possible while keeping the heat flux constant at either 20 kW/m^2, 50 kW/m^2 or 80 kW/m^2. The lines connected the data points assist with the interpretation of the experimental data and are generated by connecting the average of each collection of data points taken at a particular film flow rate.

Gewa-KS

The dryout performance of the Gewa-KS tube is illustrated in **Figure 12** at 5°C for both uncoated and coated tubes. All of the dryout profiles shared a common shape, with HTCs initially remaining constant as the film flow rate was decreased from a high point, creating the characteristic plateau. Thereafter, as film flow rate was further decreased, a gradual decline in HTCs was seen to occur from approximately 0.07 kg/m/s, or film Reynolds number of 1100.

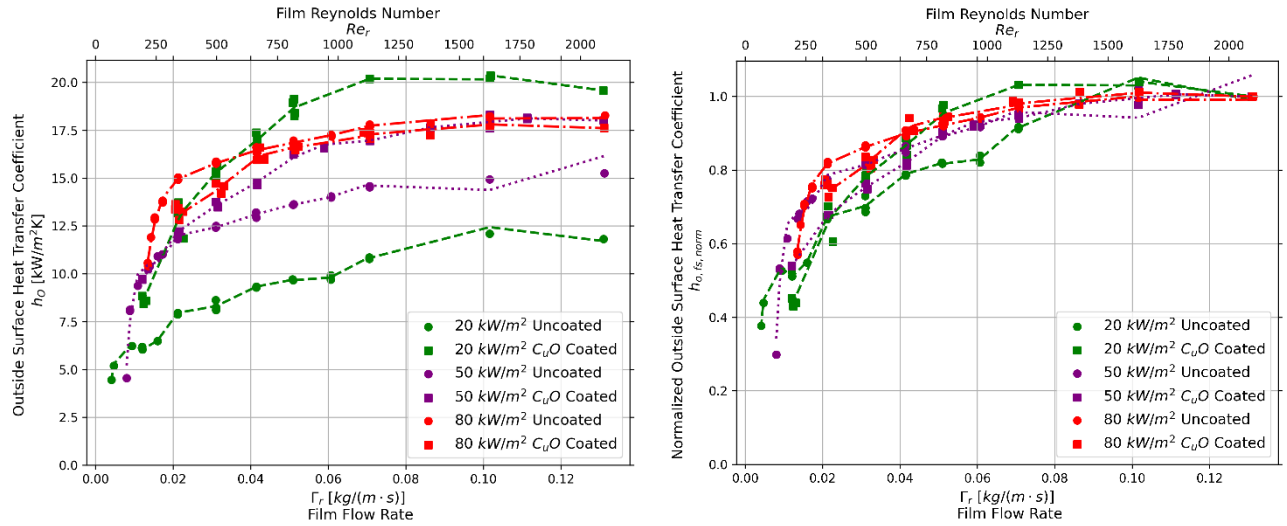

(a) HTC (b) Normalised HTC

Figure 12. Uncoated and coated Gewa-KS tube dryout performance as film flow rate is varied at 5°C saturation temperature at 20, 50 and 80 kW/m^2.

Considering the normalized data illustrated in **Figure 12** (b), the dryout profiles are all very similar for both the uncoated and coated tubes and across all three heat fluxes tested. The coating was theorized to be able to improve the dryout performance, but these results do not indicate that the CuO coating was able to improve dryout on the Gewa-KS tube. Increased heat flux is known to worsen dryout performance in previous studies of plain and 3D enhanced surfaces [9, 42], but **Figure 12** (b) results show that heat flux did not have a discernible influence on the dryout performance. This suggests that the low-finned microstructures on the Gewa-KS tube were perhaps the dominant

factor influence dryout, with the fins prevent the axial spreading of liquid along the length of the tube, resulting in the worsening of the dryout performance. The fins thus likely worsened the dryout performance before heat flux influences could play a part.

Gewa-B5

The dryout performance of the uncoated and coated Gewa-B5 tubes at 5°C is illustrated in **Figure 13**. The dryout profiles consist of a large flat plateau region with HTCs remaining constant as the film flow rate is decreased at all heat fluxes tested. The plateau region is notably larger than that of the Gewa-KS tube, with the HTCs dropping between approximately 0.01 kg/m/s to 0.03 kg/m/s or film Reynolds number of 150 to 500.

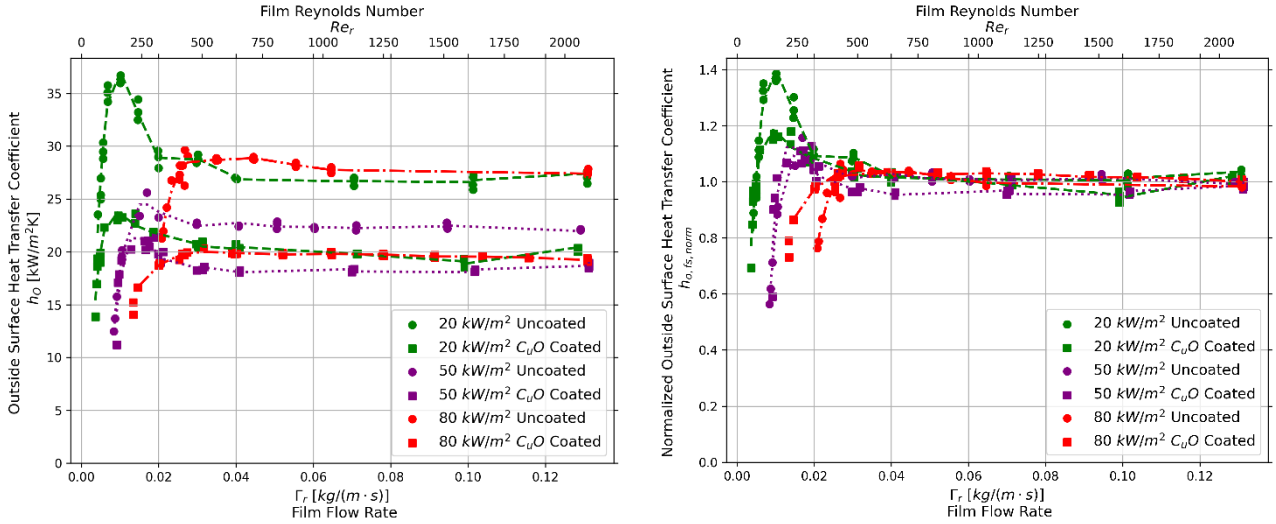

(a) HTC (b) Normalised HTC

Figure 13. Uncoated and coated Gewa-B5 tube dryout performance as film flow rate is varied for 5°C saturation temperature at 20, 50 and 80 kW/m²

The HTCs of the dryout profile at 20 kW/m², and to a lesser extent at 50 kW/m², are seen to increase at the end of the plateau region as film flow rate is decreased for both the coated and uncoated tubes. This HTC 'hump' has been noted in previous studies[9, 14, 16] is thought to be a thin film evaporation process, as a result of tube surface maintaining a intact thin film at the low film flow rate. This only occurs on tubes with improved wettability that can maintain the very thin liquid film without dryout occurring. The thin liquid layer is then superheated and boosts evaporation to the point that is can meaningfully contribute to the overall heat flux and boost the heat transfer process. This process is only achievable if a very thin liquid layer can be sustained, which explains why at 80 kW/m², no such HTC 'hump' is seen.

All dryout profiles, either after the HTC 'hump' as the film flow rate is decreased, or simply at the end of the plateau region, then experience critical dryout where a steep HTC drop is seen as dryout becomes dominant on the tube surface. Comparing the critical dryout point at the three heat fluxes tested, it is clear that as the heat flux is increased, the critical dryout point occurs at a higher film flow rate.

If comparing the uncoated to coated tube dryout performance, particularly using the normalised results of **Figure 13** (b), the CuO coating is not seen to have any influence on the dryout profile at 20 kW/m² and 50 kW/m². At 80 kW/m² the coated Gewa-B5 does experience critical dryout at a lower film Reynolds number, but the influence is considered small. Thus, the CuO coating did not have the hoped-for effect of improving the dryout performance significantly on the Gewa-B5 tube.

Turbo EHPII

The dryout performance of the Turbo EHPII tubes is shown in **Figure 14** for 5°C. Both the uncoated and coated tubes showed the distinctive plateau region as the film flow rate was decreased. Similar to the Gewa-B5 tube, the Turbo EHPII has a HTC 'hump' 20 kW/m² and 50 kW/m² as the film flow rate is further decreased beyond the plateau region.

The CuO coating again did not produce a noted improvement in dryout performance, with the normalised data of **Figure 14** (b) showing that the coated tube had a lower critical dryout threshold at 20 kW/m², at 50 kW/m² similar critical dryout threshold were reached, and at 80 kW/m² the uncoated tube had the lower critical dryout threshold. These differences though are not considered substantial.

Critical dryout occurred at higher film flow rates as heat flux was increased for the Turbo EHPII tubes, as was for the Gewa-B5 tube.

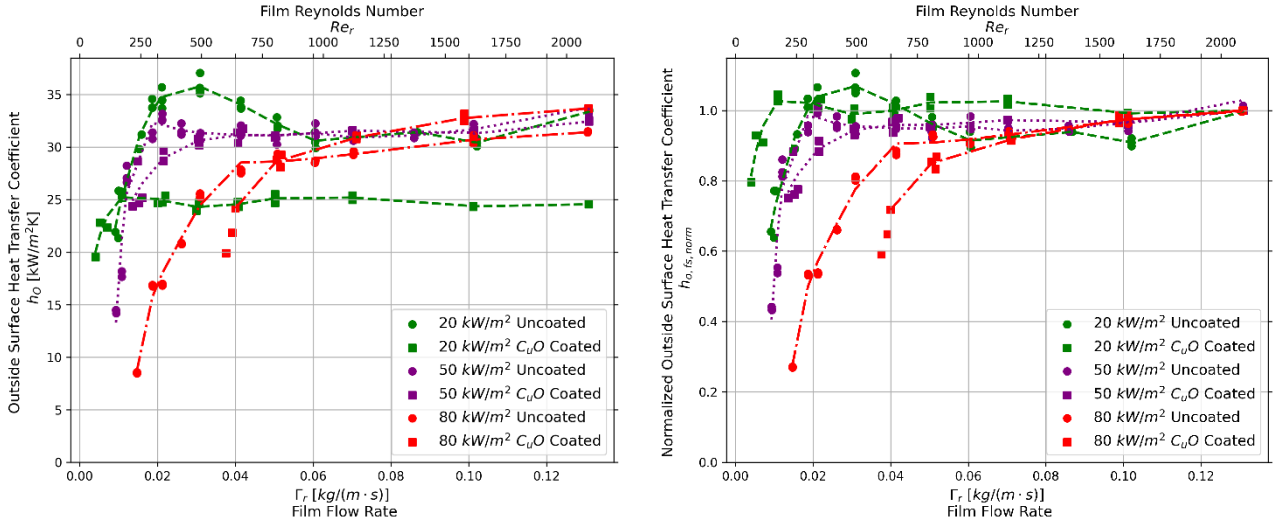

(a) HTC (b) Normalised HTC

Figure 14. Uncoated and coated Turbo EHPII tube dryout performance as film flow rate is varied for 5°C saturation temperature at 20, 50 and 80 kW/m²

4.5. Discussion of dryout performance of micro and nano scale enhancements

The microscale enhanced tubes had varying dryout performances, highlighting the ability of microscale structures to significantly effect dryout in falling film boiling. Comparing the low-finned Gewa-KS, the Gewa-B5 and the Turbo EHPII tube, it is clear the Gewa-B5 had the best dryout performance, followed by the Turbo EHPII and lastly the Gewa-KS tube. The open pore structure of the Gewa-B5 likely contributed to its improved dryout performance. The open pore structure would allow for fluid more easily be supplied to areas beginning to experience dryout and possibly also holds more liquid up, compared to the Turbo EHPII's closed off pores. The Gewa-KS's fins are sure to be the root cause of its poor dryout performance, with lateral distribution of liquid not possible due to their presence.

The nanostructures however were shown to have insignificant influence on the dryout profiles of the tubes. Their influence on wettability under these boiling conditions thus appears to be minimal, even with the ability to wick the refrigerant. While Jin et al. [17] attempted the opposite of this study and applied a polymeric coating on tube surfaces to decrease the wettability, they similarly found that attempting to change the wettability of low surface tension fluids such as refrigerants and fluorinerts on metals a challenge.

Thus, microscale enhancements, that are able to trap and distribute liquids on the tube surface, all the while enhancing heat transfer, appear to be the most fruitful area of research going forward to reduce dryout in refrigerant falling film evaporators.

5. Conclusions

This study experimentally investigated the heat transfer performance of roughened plain, low finned and two 3D enhanced tubes under falling film boiling of R-134a refrigerant at 5°C and 25°C saturation temperatures. The tubes were tested uncoated as well as coated with a CuO nanostructure across a range of heat fluxes and film flow rates.

The following key conclusions can be drawn from the study:

1. The uncoated 3D enhanced Turbo EHPII and Gewa-B5 tubes obtained the highest HTCs, outperforming an uncoated roughened plain tube by up to 500 % at 5°C.
2. The application of the CuO coating decreased the HTCs of the roughened plain tube and 3D enhanced tubes by between 10 to 40 % across the heat flux range tested, except for the Turbo EHPII tube above 60 kW/m².

3. The low finned Gewa-KS benefitted from the application of the CuO nanocoating, as well as from the falling film mode of operation when compared to pool boiling. The bubbles sliding in the fin channels and the CuO nanocoating further wicking liquid underneath these bubbles is thought to have caused this.
4. The CuO nanocoating was not shown to significantly improve the dryout performance of any of the tubes tested at either 5 or 25°C.
5. The Gewa-B5 tubes have the best dryout performance, followed by the Turbo EHPII tubes and then the low finned Gewa-KS tube, whether coated or not. The open pore structure of the Gewa-B5 likely aided it in dryout prevention, while the fins of the Gewa-KS are thought to have prevented lateral fluid distribution.

Microstructure enhancements were proven in this study to have significant influence on heat transfer and dryout performance, and it is recommended that future focus is given to optimising microscale enhancements that improve not only boiling heat transfer but also dryout performance.

Future research should also consider other coatings that may improve heat transfer and dryout in falling film boiling flows, but coatings that produce rough surface structures within the channels of 3D enhanced tubes should be avoided due to the expected heat transfer degradation.

Credit authorship contribution statement

Bradley D. Bock: Conceptualisation, methodology, formal analysis, resources, writing – original draft, supervision, project administration. **Dian Dickson:** Validation, formal analysis, investigation, data curation, visualisation, writing – review & editing. **John R. Thome:** Methodology, resources, supervision, writing – review and editing.

Declaration of competing interest

The authors declared that there is no conflict of interest.

Acknowledgements

The authors express their gratitude to the Renewable Energy Hub and Spokes Programme of the Department of Science and Innovation (DSI) for funding received, and Wieland Group for the supply of the tubes tested.

References

1. Thome, J.R., *Engineering data book 3.* Wolverine Tube Inc, 2004.
2. Ziviani, D., et al., *Analysis of an organic Rankine cycle with liquid-flooded expansion and internal regeneration (ORCLFE).* Energy, 2018. **144**: p. 1092-1106.
3. Ashwni and A.F. Sherwani, *Analysis of solar energy driven organic Rankine cycle-vapor compression refrigeration system.* Thermal Science and Engineering Progress, 2022. **35**: p. 101477.
4. Ribatski, G. and A.M. Jacobi, *Falling-film evaporation on horizontal tubes - A critical review.* International Journal of Refrigeration, 2005. **28**(5): p. 635-653.
5. Kim, D.E., et al., *Review of boiling heat transfer enhancement on micro/nanostructured surfaces.* Experimental Thermal and Fluid Science, 2015. **66**: p. 173-196.
6. Li, X., I. Cole, and J. Tu, *A review of nucleate boiling on nanoengineered surfaces: The nanostructures, phenomena and mechanisms.* International Journal of Heat and Mass Transfer, 2019. **141**: p. 20-33.
7. Zheng, Y., et al., *Experimental study of falling film evaporation heat transfer on superhydrophilic horizontal-tubes at low spray density.* Applied Thermal Engineering, 2017. **111**: p. 1548-1556.
8. Köroğlu, B., K.S. Lee, and C. Park, *Nano/micro-scale surface modifications using copper oxidation for enhancement of surface wetting and falling-film heat transfer.* International Journal of Heat and Mass Transfer, 2013. **62**: p. 794-804.
9. Bock, B.D., et al., *Falling film boiling of refrigerants over nanostructured and roughened tubes: Heat transfer, dryout and critical heat flux.* International Journal of Heat and Mass Transfer, 2020. **163**: p. 120452.
10. Bock, B.D., et al., *Pool boiling of refrigerants over nanostructured and roughened tubes.* International Journal of Heat and Mass Transfer, 2020. **162**: p. 120387.
11. Thome, J.R., *Enhanced boiling heat transfer*. 1990: Taylor & Francis.
12. Rahman, M.M., et al. *Investigation of pool boiling heat transfer and CHF enhancement on nano-engineered surfaces using advanced diagnostics*. in *International Conference on Boiling and Condensation Heat Transfer*. 2018. Nagasaki, Japan.

13. Chien, L.-H. and Y.-L. Tsai, *An experimental study of pool boiling and falling film vaporization on horizontal tubes in R245fa.* Applied Thermal Engineering, 2011. **31**(17–18): p. 4044-4054.
14. Jin, P.-H., et al., *Experimental study of falling film evaporation in tube bundles of doubly-enhanced, horizontal tubes.* Applied Thermal Engineering, 2020. **170**: p. 115006.
15. Ubara, T., H. Asano, and K. Sugimoto, *Heat transfer enhancement of falling film evaporation on a horizontal tube by thermal spray coating.* Applied Sciences, 2020. **10**(5): p. 1632.
16. Zhao, C.-Y., et al., *Experimental investigations of R134a and R123 falling film evaporation on enhanced horizontal tubes.* International Journal of Refrigeration, 2017. **75**: p. 190-203.
17. Jin, P.-H., et al., *Liquid film boiling on plain and structured tubular surfaces with and without hydrophobic coating.* International Communications in Heat and Mass Transfer, 2021. **125**: p. 105284.
18. Chen, J., et al. *Falling film evaporation of refrigerants*. in *Institution of Chemical Engineers Symposium Series*. 1994. HEMSPHERE PUBLISHING CORPORATION.
19. Moeykens, S.A. and M.B. Pate, *The effects of nozzle height and orifice size on spray evaporation heat transfer performance for a low-finned, triangulaRpitch tube bundle with R134a*. 1995, American Society of Heating, Refrigerating and Air-Conditioning Engineers, Inc., Atlanta, GA (United States).
20. Liu, B., et al., *Pool boiling heat transfer of n-pentane on micro/nanostructured surfaces.* International Journal of Thermal Sciences, 2018. **130**: p. 386-394.
21. Liang, G. and I. Mudawar, *Review of pool boiling enhancement by surface modification.* International Journal of Heat and Mass Transfer, 2019. **128**: p. 892-933.
22. Chu, K.-H., et al., *Hierarchically structured surfaces for boiling critical heat flux enhancement.* Applied Physics Letters, 2013. **102**(15): p. 151602.
23. Rahman, M.M., E. Ölçeroğlu, and M. McCarthy, *Role of wickability on the critical heat flux of structured superhydrophilic surfaces.* Langmuir, 2014. **30**(37): p. 11225-11234.
24. Liu, B., et al., *Enhanced pool boiling on micro-nano composited surfaces with nanostructures on micro-pin-fins.* International Journal of Heat and Mass Transfer, 2022. **190**: p. 122812.
25. Deng, D., et al., *Pool boiling heat transfer of porous structures with reentrant cavities.* International Journal of Heat and Mass Transfer, 2016. **99**: p. 556-568.
26. Dickson, D., B.D. Bock, and J.R. Thome, *Heat transfer of nanostructure coated commercially micro-enhanced refrigeration tubes under pool boiling conditions.* Applied Thermal Engineering, 2023. **Submitted : Manuscript number ATE-D-23-03527**.
27. Bock, B.D., J.P. Meyer, and J.R. Thome, *Falling film boiling and pool boiling on plain circular tubes: Influence of surface roughness, surface material and saturation temperature on heat transfer and dryout.* Experimental Thermal and Fluid Science, 2019. **109**: p. 109870.
28. Bock, B.D., *Surface influences on falling film boiling and pool boiling of saturated refrigerants*. 2020, University of Pretoria: Pretoria, South Africa.
29. Nam, Y. and Y.S. Ju, *A comparative study of the morphology and wetting characteristics of micro/nanostructured Cu surfaces for phase change heat transfer applications.* Journal of Adhesion Science and Technology, 2013. **27**(20): p. 2163-2176.
30. Enright, R., et al., *Condensation on Superhydrophobic Copper Oxide Nanostructures.* Journal of Heat Transfer, 2013. **135**(9).
31. Gnielinski, V., *New equations for heat and mass-transfer in turbulent pipe and channel flow.* International Chemical Engineering, 1976. **16**(2): p. 359-368.
32. Petukhov, B.S., *Heat transfer and friction in turbulent pipe flow with variable physical properties*, in *Advances in Heat Transfer*, J.P. Hartnett and T.F. Irvine, Editors. 1970, Elsevier. p. 503-564.
33. Bell, I.H., et al., *Pure and Pseudo-pure Fluid Thermophysical Property Evaluation and the Open-Source Thermophysical Property Library CoolProp.* Industrial & Engineering Chemistry Research, 2014. **53**(6): p. 2498-2508.
34. Dunn, P.F., *Measurement and data analysis for engineering and science*. 2nd ed. 2010: CRC press.
35. BIPM, I., et al., *Evaluation of measurement data—guide to the expression of uncertainty in measurement, JCGM 100: 2008 GUM 1995 with minor corrections.* Joint Committee for Guides in Metrology, 2008.
36. Christians, M. and J.R. Thome, *Falling film evaporation on enhanced tubes, part 1: Experimental results for pool boiling, onset-of-dryout and falling film evaporation.* International Journal of Refrigeration, 2012. **35**(2): p. 300-312.
37. Roques, J.F. and J.R. Thome, *Falling films on arrays of horizontal tubes with R134a, part 1: Boiling heat transfer results for four types of tubes.* Heat Transfer Engineering, 2007. **28**(5): p. 398-414.
38. Zhao, C.-Y., et al., *Experimental study of the local and average falling film evaporation coefficients in a horizontal enhanced tube bundle using R134a.* Applied Thermal Engineering, 2018. **129**: p. 502-511.
39. Lienhard, J. and V.K. Dhir, *Extended hydrodynamic theory of the peak and minimum pool boiling heat fluxes.* NASA Report CR-2270, 1973.

40. Zhao, C.-Y., et al., *Heat transfer correlation of the falling film evaporation on a single horizontal smooth tube.* Applied Thermal Engineering, 2016. **103**(Supplement C): p. 177-186.
41. Ji, W.-T., et al., *Falling film evaporation and nucleate pool boiling heat transfer of R134a on the same enhanced tube.* Applied Thermal Engineering, 2019. **147**: p. 113-121.
42. Ueda, T., M. Inoue, and S. Nagatome, *Critical heat flux and droplet entrainment rate in boiling of falling liquid films.* International Journal of Heat and Mass Transfer, 1981. **24**(7): p. 1257-1266.